Chapter 7

Fundamentals of Electrochemistry with Application to Direct Alcohol Fuel Cell Modeling

Juan Sánchez-Monreal, Marcos Vera and
Pablo A. García-Salaberri

Additional information is available at the end of the chapter

http://dx.doi.org/10.5772/intechopen.71635

Abstract

Fuel cell modeling is an inherently multiphysics problem. As a result, scientists and engineers trained in different areas are required to work together in this field to address the complex physicochemical phenomena involved in the design and optimization of fuel cell systems. This multidisciplinary approach forces researchers to become accustomed to new concepts. Electrochemical processes, for example, constitute the heart of a fuel cell. Accurate modeling of electrochemical reactions is therefore essential to successfully predict the performance of these devices. However, becoming familiar with the complex concepts of electrochemistry can be an arduous task for those who approach the study of fuel cells from fields other than chemical engineering. This process can extend over time and requires careful reading of many textbooks and papers, the most illuminating ones being hidden to the newcomer in a plethora of recent publications on the subject. The authors, who engaged in the study of fuel cells coming from the field of mechanical engineering, had to travel this road once and, with this contribution, would like to make the journey easier for those who come behind. As an illustrative example, the thermodynamic and electrochemical principles reviewed in this chapter are applied to a complex electrochemical system, the direct ethanol fuel cell (DEFC), reviewing recent work on this problem and suggesting future research directions.

Keywords: PEM fuel cells, direct alcohol fuel cells, fuel cell modeling, electrochemistry, reaction mechanisms

1. Introduction

A fuel cell is an electrochemical device that converts the chemical energy stored in a fuel and an oxidant directly into electricity, heat, and reaction products. The electric current is generated by a pair of *redox* reactions that occur separated by an *electrolyte*. At the anode, the fuel is oxidized,

generating electrons and ions, while at the cathode the oxidant is reduced, consuming the electrons and ions generated at the anode. The electrolyte is specifically designed so that it cannot conduct electrons, which flow through an external circuit performing electrical work, while it allows the flow of ions needed to maintain global electrical neutrality. Unlike conventional batteries, fuel cells require that the fuel and the oxidant be supplied continuously to sustain the electrochemical reactions.

The operation of a fuel cell is driven by chemical processes. As a result, these devices circumvent the Carnot cycle limitations of thermal devices and the mechanical limitations of systems with moving parts. In addition, the amount of electrical energy that can be generated by a fuel cell is only limited by the capacity of the fuel and oxidant reservoirs, which eliminates the long recharge times characteristic of conventional batteries.

The discovery of the fuel cell operating principle is commonly attributed to Sir William R. Grove [1], who also invented a practical device based on this principle: the so-called *gaseous voltaic battery* [2]. Recent work, however, attributes the discovery to Christian Friedrich Schöenbein, the famous German-Swiss chemist, better known for his discoveries of guncotton and ozone, a year before Sir William R. Grove [3]. It is well known that both scientists maintained a lively scientific correspondence, which may be the origin of the confusion. Anyway, until the introduction of PTFE (Teflon) in 1950s, fuel cells were rather a scientific curiosity than a practical system.

The first practical application of fuel cells was in space. The National Aeronautics and Space Administration (NASA) used them in the Gemini program during the 1950s and later in the Apollo program. The first mission that used a fuel cell was an unmanned suborbital flight on October 30, 1960. The Gemini module launched in that mission mounted the first alkaline fuel cell developed by General Electric, which generated 1 kW power with 29 kg weight and provided a potable water source for the crew of future manned missions. During the Apollo program, NASA used the alkaline fuel cells developed by Pratt & Whitney based on Sir Francis T. Bacon patents [4, 5]. However, it was not until 1990s when the industry (Ballard, Plug Power, etc.) started the development of commercial fuel cells, mainly for automotive and backup power applications, and the US Department of Energy included fuel cells among its main research interests.

Fuel cells are often classified by the type of electrolyte they use, because the charge transport process that occurs in the electrolyte determines drastically the electrochemical reactions that take place in the cell, the kind of catalysts required, the temperature range in which the cell operates, the potential fuels, and other factors. These characteristics, in turn, affect the applications for which the different types of fuel cells are most suitable. According to the Fuel Cell Technologies Office Multi-Year Research, Development, and Demonstration (MYRD&D) Plan [6], the largest markets for fuel cells today are in stationary power, portable power, auxiliary power units, backup power, and material handling equipment. Among fuel cell end users, the automotive sector stands out as one of the most relevant ones [7, 8]. However, there are still some barriers for the development of fuel cells, both technical and economical [6]. The use of catalysts is mandatory to reach competitive power densities, as they significantly accelerate the electrochemical reactions. In low-temperature fuel cells, the catalysts are usually based on

noble metals, such as platinum, which are scarce and very expensive. The electrolyte is also one of the main challenges. It often requires strict working conditions (in terms of temperature, humidity, etc.) to operate properly. As well, fuels and oxidants are not always easy to manage or store, which significantly increases system complexity.

The present volume is devoted to proton exchange membrane (PEM) fuel cells, whose particularities are summarized in Section 2. The specific topics of this chapter are addressed next. A brief summary of the overall performance of PEM fuel cells (PEMFCs) is presented in Section 3. Thermodynamic and electrochemical principles of PEM fuel cells are discussed in Sections 4 and 5. And a particular example of application of these principles to the modeling of multistep electrochemical reactions in direct alcohol PEM fuel cells is given in Section 6. Finally, the main conclusions are drawn in Section 7.

2. Proton exchange membrane fuel cells

PEM fuel cells (PEMFCs) use a polymeric electrolyte membrane to separate the anode from the cathode. As previously discussed, the polymer electrolyte membrane allows the transport of protons, but it is impermeable to electrons. The membrane is made of ionomers (synthetic polymers with ionic properties), the most extended one being Nafion®, discovered in the late 1960s by Walther Grot of DuPont. It contains perfluorovinyl ethers terminated by sulfonic acids with hydrophobic tetrafluoroethylene (Teflon) flexible structures. So the proton conductivity is achieved because the water into the membrane ionizes the acidic groups [9, 10]. The sulfonic groups -SO_3H (with general formula R-$S(=O)_2$-OH, where R represents the generic chain where the group is attached) are highly hydrophilic and can adsorb large amounts of water, creating hydrated regions. In these regions, the H^+ are weakly attracted by the SO_3^- groups, which are rigidly attached to the Teflon structure, and they are able to move easily. The hydrated hydrophilic regions thus behave as dilute acids, explaining why the membrane needs to be well hydrated for the proton conductivity to be appreciable. Both the polymeric nature of the membrane and the requirement of membrane hydration restrict the operational temperature range between 60 and 90°C, although air-breathing or passive systems may operate even at room temperature.

The transport of protons in the membrane forces the electrochemical reactions to produce or consume protons as charge carriers. At the anode side, the most extended fuel in PEMFCs is hydrogen [7], although alcohols are also used in direct alcohol fuel cells (DAFCs). The use of alcohols generates significantly less power than hydrogen, but they offer safer operation for unattended low-power missions. At the cathode side, oxygen is reduced with the protons and electrons released in the anode to generate water as only reaction product. As previously discussed, the protons reach the cathode crossing the membrane, whereas the electrons are conducted through an external circuit generating current. The oxygen can be supplied as a pure gas or diluted as part of an air stream feed directly to the cell.

To optimize the power output of PEMFCs operated with hydrogen, adequate operating conditions are needed. Most PEMFCs operate between 60 and 80°C to exploit the proton conductivity

of the membrane. Proper humidification of the gas feed streams is often used to guarantee an adequate membrane water content. The hydrogen and air streams are usually pressurized (typically at 0.5 bar gauge pressure) to facilitate water management [11]. To provide these cell conditions, additional systems are required. However, other operating conditions have also been investigated to try to eliminate auxiliary systems. Passive fuel cells rely on natural mechanisms, such as capillary forces, diffusion, convection, and evaporation, to achieve cell feeding without extra power consumption. Among the passive systems used, one finds air-breathing systems for the anode electrode [12], pressurized cannisters [13], and capillary liquid systems [14]. There are also passive cells running on different fuels, such as hydrogen [12, 15, 16], methanol [17], and ethanol [18]. In general, passive systems are more suitable for portable power sources [19]. In the last decade, microbial fuel cells (MFCs), which use bacteria as the catalysts to oxidize organic and inorganic matters, have also been developed with application to microdevices [20].

High-temperature polymer exchange membrane fuel cells (HT-PEMFCs) are another variant of PEMFCs. They operate between 100 and 200°C, are able to run in dry conditions, and tolerate impure fuel streams (e.g., hydrogen obtained from reforming gases), and the excess heat can be used for cogeneration. These characteristics can be exploited to simplify the system design, which increases its overall efficiency. Nevertheless, materials other than Nafion must be used for the membrane (PBI, SPEEK, SPI, or SPSV) and the proton carrier (phosphoric acid or ionic liquids) [21, 22]. High-temperature operation has also been considered for DAFCs [23–25] to improve the effectiveness of the C–C bond breaking step in higher alcohols such as ethanol.

2.1. Direct alcohol PEM fuel cells

In addition to hydrogen, several liquid organic and inorganic compounds can be used as fuels in PEMFCs [26]. Common inorganic compounds tested for use are ammonia, hydrazine, borohydrides, and ammonia borane. Among the organic compounds used, there are alcohols, hydrocarbons, acids, and glycol compounds. Most of the organic compounds tested are produced by renewable biomass sources, which makes them a suitable clean option. Besides PEM membranes, also anion exchange membranes (AEMs) are used in alkaline cells [27]. Liquid fuels can be used either pure or diluted for safety reasons. Water is the most used solvent due to its natural properties and because of its importance for the correct operation of the membrane. Alcohols are considered a promising source fuel to fuel cells [28]. Light alcohols, such as methanol or ethanol, are able to electrooxidate at relative low temperatures (less than 90°C). They also have a higher energy density than hydrogen. The electrooxidation of alcohols consumes water, which makes water an optimum solvent for the fuel supply. In addition, aqueous alcohol solutions are typically fed at low concentrations (0.5–2 M), which makes their operation and storage safer. These advantages make DAFCs an alternative option for low-power applications such as portable devices or unattended remote stations. Furthermore, more complex alcohols (e.g., propanol isomers, 2-methylpropan-2-ol, and butan-2-ol) may be an option at higher temperatures (up to 300°C). Nacef et al. [29] carried out an extensive thermodynamic study about the potential performances of several alcohols used in PEM fuel cells.

Nevertheless, some disadvantages arise when alcohols are used in PEM fuel cells. Contrary to hydrogen, alcohol electrooxidation is a sluggish process that involves many elementary reactions

generating high activation overpotentials. This results in a severe reduction of fuel cell performance. Besides that, since the alcohols are supplied as aqueous dilutions and the membrane is highly permeable to water, a *crossover* flux of fuel is established across the membrane. The fuel that crosses the membrane is electrooxidized at the cathode electrode, generating an undesired parasitic current that also results in larger cathode activation losses [30–37].

The electrooxidation of organic compounds is not straightforward, as it proceeds as a branched, multistep, reaction [38, 39]. Due to the large number of chemical bonds of the compounds, several reactions can be expected. Unfortunately, poisoning species such as carbon monoxide are found among the reaction intermediates that are formed in the reaction path. The CO groups remain adsorbed to the catalyst, blocking the active reaction sites. This produces a sharp reduction of the effective catalyst surface area, which also reduces cell performance [25, 40–42]. To mitigate this effect, binary Pt-based catalysts include a secondary metal, such as Sn or Ru [42–52]; the blockage of active sites is alleviated via a bifunctional mechanism that allows the absorption of hydroxyl groups at lower potentials on the secondary metal, thus favoring further oxidation of Pt-adsorbates blocking the active catalyst sites [53–55]. It is interesting to note that the problem of CO poisoning is not unique to DAFCs; low-temperature PEMFCs running on hydrogen have very low tolerance to impurities (e.g., CO) in the fuel, requiring very high purity hydrogen that is costly to produce. Fuel cells operated with reformate gas also exhibit this problem [56].

DAFCs are suitable for portable power applications (e.g., battery chargers, consumer electronics, handheld terminals, unattended security devices, notebook PCs, emergency response mobile communications, or even auxiliary power units) and material handling equipment. The power requirements for these applications are low, and the cost targets and infrastructure requirements are not as challenging as for transportation applications [6, 57].

Considering all the types of DAFCs currently under development, those running on methanol and ethanol are, in this order, the ones that have reached further progress. Below we describe the particularities of these fuel cells, indicating the main advantages and disadvantages of both.

2.1.1. Direct methanol fuel cells (DMFCs)

Methanol is the simplest alcohol. Due to the lack of the C–C bond present in higher alcohols, methanol is the alcohol with the largest number of hydrogens per carbon [58], which makes it a good hydrogen carrier. However, reforming methanol to H_2 is still under study. By contrast, a DMFC uses methanol as fuel without producing H_2 during the process. The device operates with diluted methanol (1−2 M), and only a fraction of the diluted fuel is used. The device recycles the outlet and replenishes it to keep methanol concentration [59]. Platinum-based catalysts show the best results [60]; additionally, secondary metals are included to reduce the impact of CO poisoning [39, 59, 61, 62]. As previously discussed, the main applications of DMFCs are on small portable devices: battery chargers, consumer electronics, notebook PCs, and portable generators [57, 59, 63]. Actual challenges for DMFCs marked by DOE include reducing Pt loading, reducing methanol crossover to increase efficiency, simplifying the side-on systems to increase energy and power density, improve reliability, and reduce cost [6].

2.1.2. Direct ethanol fuel cells (DEFCs)

Ethanol is a fully renewable alcohol that can be readily obtained from the fermentations of biomass and is much less toxic than methanol [27, 64]. Fuel Cell Technologies Office plans [6] include ethanol tolerance for liquid-feed fuel cells operated with fuel blends. The number of patents in DEFC is steadily growing since 2002, which suggests that DEFC technology is still under development and further progress can be expected [57]. The complete electrooxidation of ethanol to CO_2 would make DEFCs useful even for automotive purposes [27]. But the sluggish kinetics of the ethanol electrooxidation reaction hinders this achievement [27, 65–67]. By way of contrast, due to its larger molecular structure, ethanol has a lower crossover rate than methanol, which together with its slower electrochemical oxidation kinetics produces a lesser effect on the cathode performance [68, 69]. The complexity of ethanol electooxidation is originated by the difficulty of breaking the C–C bond [43, 61, 66, 70–77], a problem that is shared with other higher alcohols.

3. Performance of PEM fuel cells

The overall performance of a fuel cell is usually represented by the current density (i.e., current per unit surface) vs. voltage curve, often referred to as the *polarization curve*. Thermodynamics teaches us that, in an ideal process in which mass and charge transport phenomena occur in a reversible manner, the output voltage should remain constant independently of the current density. Such an ideal reversible voltage, or potential, E, is determined by the electrochemical reactions that occur in the cell and therefore is directly related to the redox pair. Operational parameters such as temperature and pressure also influence the ideal reversible potential.

The deviations between the ideal equilibrium potential of the redox pair and the polarization curve provide a measure of the fuel cell efficiency. The actual current density vs. voltage curve for a particular fuel cell (geometry, catalyst/electrode characteristics, and electrolyte properties) and operating conditions (reactant concentrations, flow rates, pressures, temperature, and relative humidity) is dependent on both activation (i.e., kinetic), ohmic, and mass transport losses, to be described below:

- **Activation losses** are originated by the finite rate of the electrochemical reactions that take place in the cell electrodes.
- **Mass transport losses** arise when the reactants are not supplied at the same rate than they can be consumed. Mass transport losses are dominated by the porous layers and interfacial phenomena [78]. As previously discussed, one of the main tasks of the porous layers is to smooth the channel-rib pattern of the bipolar plates to provide an as homogeneous as possible supply of reactants to the catalyst layers. However, this task entails a certain mass transfer resistance that produces significant mass transport losses at large current densities.
- **Ohmic losses** are generated by the irreversible charge transport processes associated with finite charge transport conductivities. Electrons move through the solid phase of the gas diffusion layers and other elements of the cell and their interfaces, while protons are

conducted through the polymeric membrane. Although the charge transport mechanisms are different, both result in finite voltage drops. These losses grow linearly with the current density as stated by Ohm's law.

The actual cell voltage at a given current density can then be expressed as the ideal reversible potential, E, minus the so-called activation (act), transport (transp), and ohmic (ohm) overpotentials

$$V = E - \eta_{\text{act}} - \eta_{\text{transp}} - \eta_{\text{ohm}} \tag{1}$$

However, for modeling purposes, the voltage losses are often separated by regions rather than processes

$$V = E - \eta_{\text{a}} - \eta_{\text{c}} - \eta_{\text{mem}} \tag{2}$$

where η_{a}, η_{c}, and η_{mem} denote the voltage losses (including activation, mass transport, and ohmic contributions) at the anode, the cathode, and the membrane.

Electrooxidation reactions arise as a crucial issue in DAFCs, since they largely determine both η_{a} and η_{c}. For instance, the incomplete electrooxidation of ethanol hinders the theoretical maximum energy release in direct ethanol fuel cells, while at the same time it generates a variety of partially oxidized products. An accurate DAFC model therefore has to predict current density and overpotentials as well as a detailed description of the residual products. For this purpose, a systematic formulation of the multistep electrochemical reactions that take place in DAFCs is highly desirable.

4. Thermodynamic principles of PEM fuel cells

4.1. Redox pairs

The most important driving processes that take place in a fuel cell are the electrochemical reactions between the fuel and the oxidant. As implied by the prefix *electro-*[1], these reactions involve the transfer of electric charges, and this fact is achieved through a pair of *redox* (i.e., *re*duction–*ox*idation) reactions. A *redox* reaction is separated into two half-reactions: the oxidation and the reduction reactions. In the oxidation reaction, the reactant species looses electrons. By contrast, in the reduction reaction, the reactant species gains electrons. The oxidation and reduction reactions take place in the anode and cathode electrodes, respectively.

In a fuel cell, the redox half-reactions are kept separated by an electrolyte, with the electrodes being electrically connected through an external circuit. The electrolyte is an ionic conductor, while the electrodes and the external circuit are made of good electronic conductors. This

[1]From Latin electrum, from Ancient Greek élektron, or "amber", a natural resin, which when rubbed produces static electricity.

configuration makes it possible to separate the ionic and electronic currents, the latter being used to perform electrical work through an external circuit.

As discussed above, the reactants used for the oxidation reactions in PEM fuel cells are hydrogen and alcohols, mostly methanol and ethanol. Protons are the ionic charge carrier in these cells, so the oxidation reaction must generate protons for the operation of the system. For instance, the hydrogen oxidation reaction

$$H_2 \rightarrow 2H^+ + 2e^- \tag{3}$$

generates two protons and two electrons per molecule of hydrogen consumed. This reaction occurs in the anode of low-temperature hydrogen PEMFCs, where due to its extreme simplicity the activation losses are very small. In addition to this, the catalyst, typically made of Pt-based particles [39, 79], performs better for simpler reactions such as (3). As implied by the above reaction, hydrogen electrooxidation produces no other products than charge carriers, in this case electrons and protons; hence, it is not necessary to evacuate anything else from the anode electrode, except (maybe) the heat evolved by the reaction.

For low-power portable applications, liquid-feed direct alcohol fuel cells (DAFCs) may also be used. The simplest alcohol is methanol (CH_3OH). The electrooxidation of methanol also produces electrons and protons but generates CO_2 as well and only occurs in the presence of water

$$CH_3OH + H_2O \rightarrow CO_2 + 6H^+ + 6e^- \tag{4}$$

which requires the supply of water and the evacuation of CO_2 bubbles. This introduces stronger mass transport limitations in the anode of a DMFC than in hydrogen PEMFCs, motivated in particular by the presence of the bubbles.

The methanol oxidation reaction (MOR) takes place in multiple steps [39], and some of them lead to the production of undesirable intermediate products, such as CO [25, 40–42, 56]. Due to the multiple species involved, the reaction is slower and more complex than Reaction (3), which leads to significantly lower current densities in DMFCs than in hydrogen PEMFCs. As a result, complex and expensive catalyst compositions (Pt-Ru nanoparticles supported on high surface area carbon) must be used to minimize activation losses [42–52].

Ethanol is another alcohol used in DAFCs. It is a more complex molecule (CH_3CH_2OH) with a highly stable C–C bond, which makes it even more difficult to react. It is well known that ethanol electrooxidation may proceed through multiple pathways, which includes partial oxidation to acetaldehyde, acetic acid, or methane, as well as complete oxidation to CO_2, according to the following overall reactions

$$CH_3CH_2OH \rightarrow CH_3COH + 2H^+ + 2e^- \tag{5a}$$

$$CH_3CH_2OH + H_2O \rightarrow CH_3COOH + 4H^+ + 4e^- \tag{5b}$$

$$CH_3CH_2OH + H_2O \rightarrow CO_2 + CH_4 + 4H^+ + 4e^- \tag{5c}$$

$$CH_3CH_2OH + 3H_2O \rightarrow 2CO_2 + 12H^+ + 12e^- \tag{5d}$$

While different oxidation reactions occur in PEM fuel cells depending on the fuel type, the reduction reaction is common to all of them, namely the oxygen reduction reaction (ORR)

$$O_2 + 4H^+ + 4e^- \rightarrow 2H_2O \tag{6}$$

which combines the electrons and protons produced in the anode with a molecule of oxygen to produce water.

When combining Reactions (3), (4), or (5) with Reaction (6), different global reactions can be defined for the cell:

- Hydrogen PEM fuel cells (PEMFCs)

$$H_2 + \frac{1}{2}O_2 \rightarrow H_2O \tag{7}$$

- Direct methanol fuel cells (DMFCs)

$$CH_3OH + \frac{3}{2}O_2 \rightarrow CO_2 + 2H_2O \tag{8}$$

- Direct ethanol fuel cells (DEFCs)

$$CH_3CH_2OH + \frac{1}{2}O_2 \rightarrow CH_3COH + H_2O \tag{9}$$

$$CH_3CH_2OH + O_2 \rightarrow CH_3COOH + H_2O \tag{10}$$

$$CH_3CH_2OH + O_2 \rightarrow CO_2 + CH_4 + H_2O \tag{11}$$

$$CH_3CH_2OH + 3O_2 \rightarrow 2CO_2 + 3H_2O \tag{12}$$

4.2. Electrical work and Gibbs free energy

The energy released in a fuel cell comes from the chemical energy stored in the fuel and the oxidant, which is released by the electrochemical reactions that take place in the anode and cathode electrodes. The energy released or consumed by a chemical reaction is represented by its *heat of reaction* or *enthalpy of reaction*. This value is the enthalpy change produced in a chemical reaction, and it is calculated as the difference in *formation enthalpy* between the reaction products (P) and reactants (R) at a given temperature T

$$\Delta h^0(T) = \sum_{\mathrm{P}} v_k h_k^0(T) - \sum_{\mathrm{R}} v_k h_k^0(T) \tag{13}$$

In the above expression, v_k is the stoichiometric coefficient of species k and $h_k^0(T)$ is the molar-specific formation enthalpy of species k, which can be evaluated at temperature T from its reference value at the standard temperature T_0 as follows

$$h_k^0(T) = \Delta_f h_k^0(T_0) + \left(h_k^0(T) - h_k^0(T_0)\right) \tag{14}$$

This expression shows that the molar enthalpy of a chemical compound is made up by its molar enthalpy of formation at the reference temperature $\Delta_f h_k^0(T_0)$ plus the enthalpy change associated with the state change at fixed composition $h_k^0(T) - h_k^0(T_0)$ [80]. An extended database for these thermodynamic properties, containing data for over 2000 solid, liquid, and gaseous chemical species, is provided by NASA [81].

During the chemical reactions, entropy also changes. Just like the *enthalpy of reaction* (13), the molar *entropy of reaction* at a given temperature T and pressure p is defined as

$$\Delta s(T,p) = \sum_{\mathrm{P}} v_k s_k(T,p) - \sum_{\mathrm{R}} v_k s_k(T,p) \tag{15}$$

Unlike enthalpy, entropy has no formation contribution. As established by the third law of thermodynamics, the *absolute entropy* is defined as the entropy change between the actual estate and the absolute-zero state. For crystalline substances, entropy is zero at the absolute-zero state, whereas noncrystalline substances have a nonzero value of the entropy at the absolute-zero state [80]. The value of the absolute entropy can also be obtained from the NASA library of thermodynamic data [81].

It is well known that not all the energy available in a chemical reaction can be converted to useful work. Therefore, in a fuel cell, not all the energy released by the electrochemical reactions can be converted to electrical work as a result of entropy production. The Gibbs free energy

$$G = H - TS \tag{16}$$

represents the amount of useful energy that can be used as *potential work*. In a given process, the amount of energy that can be released as potential work is the variation of the Gibbs free energy. For an isothermal process, the variation of the molar-specific Gibbs free energy reduces to

$$\Delta \mathrm{g} = \Delta h - T\Delta s \tag{17}$$

The work performed by a fuel cell is completely electrical. In general, electrical work is done when moving a charge Q through a potential difference E. In a fuel cell, the electrical work can be written as

$$W_e = nFE \tag{18}$$

where n is the number of moles of electrons transferred in the reaction per mole of fuel consumed and $F = 96485$ C/mole of electrons is Faraday's constant. Since the maximum amount of electrical work that can be obtained is the reduction of the Gibbs free energy ($W_e = -\Delta g$), the electrical reversible potential (or voltage) obtained from the cell is

$$E = \frac{-\Delta g}{nF} \tag{19}$$

The value of the electrical reversible potential at the standard conditions, $T_0 = 298$ K and $p_0 = 100$ kPa, is called the *standard reversible potential of the reaction* E_0.

As previously discussed, water is commonly produced in PEM fuel cells. Due to the low temperatures of operation ($T < 100°C$), it can be produced in both liquid and gas phases. However, the enthalpy of formation of both phases is different, the difference being the latent heat of vaporization. As a result, the formation of liquid water yields a significantly higher reaction enthalpy than that of water vapor. To decide which phase should be used for determining the potential work, we have to apply the "philosopy" of the *Gibbs free energy* calculation. This accounts for the maximum energy that can be released as work. Since the formation of liquid water releases a larger amount of energy due to the latent heat of vaporization, which is released during condensation, the use of the gas water formation enthalpy implies an incomplete account of the available energy. The value of the reaction enthalpy obtained assuming the formation of liquid water is therefore called the higher heating value (HHV), while that obtained when water vapor is formed is called the lower heating value (LHV).

Another voltage can be defined using the reaction enthalpy (13); the *thermoneutral potential* or *enthapy potential* E_{TH} is

$$E_{TH} = \frac{-\Delta h}{nF} \tag{20}$$

This potential is useful to evaluate all the available energy contained in the fuel.

The reversible potential E accounts for the decreasing of the energy due to the entrophy generation of the chemical reactions. In a fuel cell, the actual voltage V established between the electrodes is lower than the reversible potential E and the enthalpy potential E_{TH} due to the fuel cell irreversibilities. The unused energy is dissipated as heat. Then, the total heat produced by the electrochemical reactions can be simply expressed as

$$Q = I(E_{TH} - V) \tag{21}$$

where I represents the amount of current drawn from the cell. It is interesting to note that when using the LHV to evaluate the enthalpy potential E_{TH} one obtains a lower estimation of the residual heat Q than when using the HHV. The difference comes from the fact that the HHV includes also the heat released during water condensation. However, the global energy balance should remain the same in both cases as long as the latent heat of vaporization is properly accounted for [78].

4.2.1. Hydrogen potentials

The standard potential of hydrogen PEMFCs is highly dependent on the phase of water produced. The reversible potential at 25°C is 1.229 V for liquid water and 1.185 V for water vapor (**Table 1**). In both cases, the potential decreases with temperature (**Figure 1**). Below 100°C, the production of liquid water releases more energy than that of water vapor, so the

Global reaction	Standard potential @ $T_0 = 298$ K
$H_2 + \frac{1}{2}O_2 \rightarrow H_2O$ (l)	$E_0 = 1.229$ V
$H_2 + \frac{1}{2}O_2 \rightarrow H_2O$ (g)	$E_0 = 1.185$ V
$CH_3OH + \frac{3}{2}O_2 \rightarrow CO_2 + 2H_2O$ (l)	$E_0 = 1.213$ V
$CH_3CH_2OH + \frac{1}{2}O_2 \rightarrow CH_3COH + H_2O$ (l)	$E_0 = 1.049$ V
$CH_3CH_2OH + O_2 \rightarrow CH_3COOH + H_2O$ (l)	$E_0 = 1.151$ V
$CH_3CH_2OH + O_2 \rightarrow CO_2 + CH_4 + H_2O$ (l)	$E_0 = 0.889$ V
$CH_3CH_2OH + 3O_2 \rightarrow 2CO_2 + 3H_2O$ (l)	$E_0 = 1.151$ V

Table 1. Standard reversible potentials of several global reactions of interest for PEM fuel cell modeling.

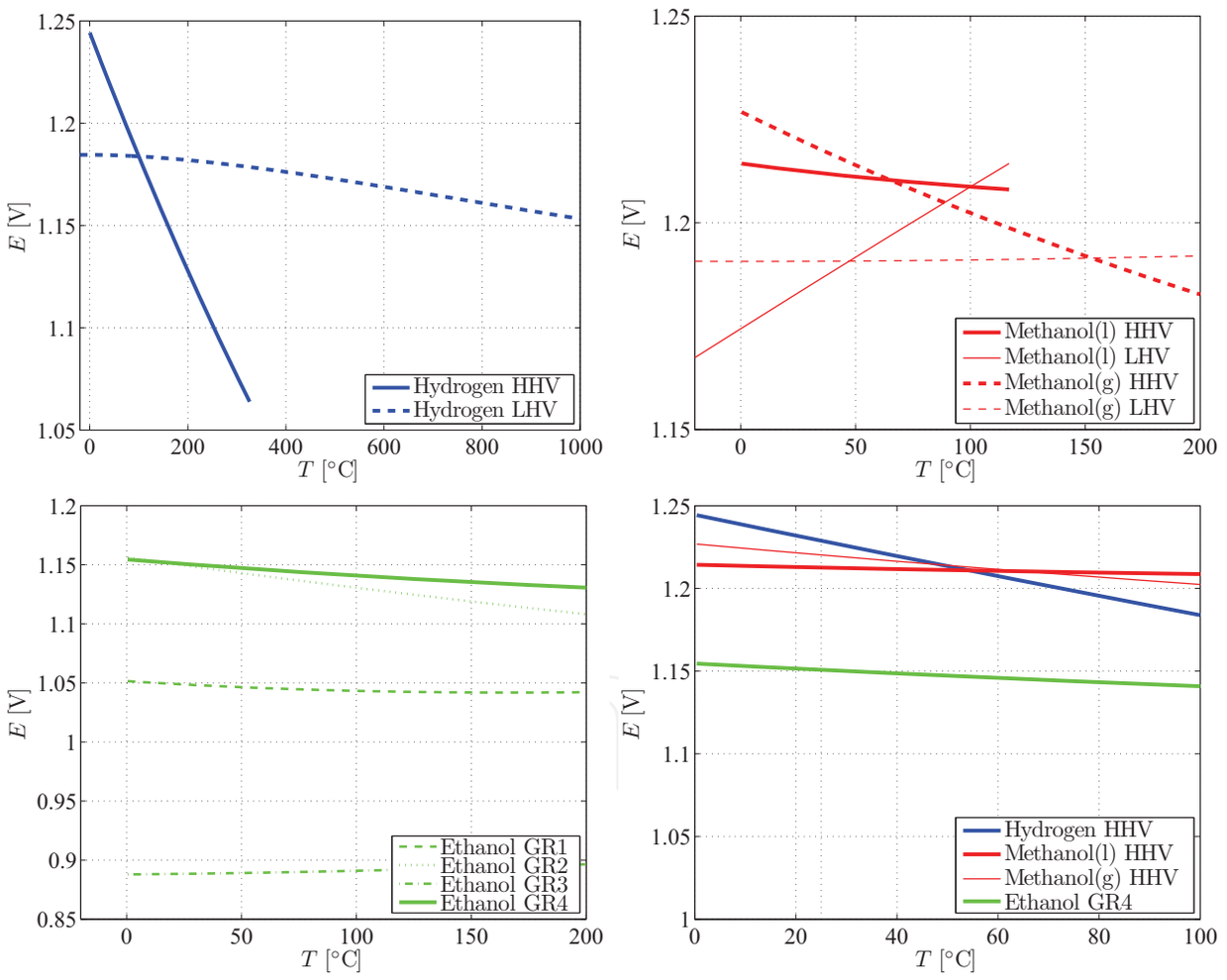

Figure 1. Reversible potentials for various global reactions of interest in PEM fuel cells.

potential evaluated using the HHV is higher in that range, whereas the potential obtained using the LHV is higher over 100°C. Low-temperature PEM fuel cells operate assuming the HHV as maximum expected energy.

4.2.2. Methanol potentials

Liquid-feed DMFCs operate at temperatures lower than 100°C, so the HHV is used for calculating their standard potential. At higher temperatures, the phase of methanol also needs to be considered. **Figure 1** shows the evolution of the standard potential for both liquid and gas methanol and water. The potential predicted assuming both species in liquid phase decreases sightly with temperature, while that obtained for gas phase is seen to increase with temperature. This fact is the basis to explore the posibility of using DMFCs at temperatures above 100°C [29].

4.2.3. Ethanol potentials

The ethanol electrooxidation reaction in DEFCs has very complex kinetics with different products [43, 61, 66, 70–77]. **Table 1** shows the global reactions considered in this study (Section 4.1). It is seen that the complete oxidation to CO_2 has the higher reversible potential, which decreases monotonically with temperature as shown in **Figure 1**. Although complete oxidation to CO_2 is difficult to achieve, the reversible potential of this reaction is often used as reference for DEFC models.

4.3. The Nernst equation

So far, the effect of reactant and product concentrations on reversible cell potential has been ignored. To understand this effect, we must introduce the chemical potential. The chemical potential of species k is defined as

$$\mu_k = \left(\frac{\partial G}{\partial n_k}\right)_{T,p,n_{l\neq k}} \tag{22}$$

and represents the change of the Gibbs free energy produced by a change in the number of moles, n_k, of species k. Thermodynamics teaches us that the Gibbs free energy of a mixture can be expressed as the sum of the chemical potentials of all the species composing the mixture

$$G = \sum_k n_k \mu_k \tag{23}$$

and that the chemical potential of species k can be expressed as

$$\mu_k = \mu_k^0 + RT \ln a_k \tag{24}$$

in terms of the activity of species k, defined as:

$$a_k = \begin{cases} p_k/p_0 & \text{ideal gases} \\ C_k/C_0 \quad \text{for} & \text{ideal dilute solutions} \\ 1 & \text{pure components} \end{cases} \tag{25}$$

where $C_0 = 1$ M is the reference concentration.

The variation of the molar-specific Gibbs free energy can then be written in terms of the chemical potentials

$$\Delta \mathrm{g} = \sum_{\mathrm{P}} \upsilon_k \mu_k^0 - \sum_{\mathrm{R}} \upsilon_k \mu_k^0 + RT \ln \frac{\prod_{\mathrm{P}} a_k^{\upsilon_k}}{\prod_{\mathrm{R}} a_k^{\upsilon_k}} \tag{26}$$

where the variation of the chemical potentials in standard conditions can be written as the standard change in the Gibbs free energy Δg^0 for the reaction

$$\Delta g = \Delta g^0 + RT \ln \frac{\prod_{\mathrm{P}} a_k^{\upsilon_k}}{\prod_{\mathrm{R}} a_k^{\upsilon_k}} \tag{27}$$

Using this expression to evaluate the reversible potential of the reaction E using Eq. (19), one obtains the *Nernst equation*

$$E = E^0 - \frac{RT}{nF} \ln \frac{\prod_{\mathrm{P}} a_k^{\upsilon_k}}{\prod_{\mathrm{R}} a_k^{\upsilon_k}} \tag{28}$$

which relates the reversible potential E of the electrochemical reaction to the standard reversible potential E^0, temperature, and activities, expressed in terms of concentrations or partial pressures. Eq. (28) owes its name to the German chemist Walther Nernst[2], who originally obtained it exclusively from experimental work [83, 84], although his equation was later deducted from first thermodynamic principles, as has been shown here.

5. Electrochemical principles of PEM fuel cells

The *key point* to the operation of a fuel cell is that the total reaction is split into two half-reactions that take place separately in the anode and cathode electrodes. The Nernst equation (28) applies to the global reaction and serves to determine the ideal reversible potential, E, but a deeper understanding requires to study both half-reactions independently. Obviously, they are electrochemical reactions as they involve electron transfer. In 1905, Julius Tafel proposed an empirical equation that related the current density j produced by an electrochemical reaction to the so-called overpotential $\eta = E - E^\star$, defined as the difference between the applied potential E and the equilibrium potential $E^\star$ [85]. This equation is commonly known as the *Tafel equation* and is customarily written in the form

$$\eta = a + b \log j \quad \text{with} \quad b = \frac{2.3RT}{\alpha F} \tag{29}$$

[2] A detailed review of the historical development of Nernst equation can be found in Ref. [82]

where α is the so-called charge transfer coefficient, whose value must be between 0 and 1, and log indicates decimal logarithm. This equation is widely used in electrochemistry and can be applied in several conditions [86].

Although Tafel obtained its equation purely by experimental methods, in the 1930s Butler and Volmer (and coworkers) derived it from the Arrhenius equation for the rate constant of a chemical reaction, rewriting the activation energy in terms of the Gibbs free energy of activation and the cell overpotential as discussed below.

5.1. From Tafel equation to Butler-Volmer equation

In 1889, Arrhenius [87][3] proposed that the temperature dependence of the rate constant of a chemical reaction could be expressed as

$$\mathfrak{K} = A \exp\left(\frac{-\Delta_A E}{RT}\right) \tag{30}$$

where T is the absolute temperature, A is the frequency factor, and $\Delta_A E$ is the activation energy. The frequency factor gives the frequency of collisions between reactant molecules. The activation energy can be defined as the change in internal energy from the reactant state to the *activated complex* state, so it is also called the *internal energy of activation*.

Since all the reactions in a fuel cell can be considered as condensed-phase reactions,[4] the *enthalpy of activation* is approximately equal to the activation energy, so that

$$\mathfrak{K} = A \exp\left(\frac{-\Delta_A H}{RT}\right) \tag{31}$$

Rewriting now the parameter A as the product $A' \exp\left(-\Delta_A S/R\right)$ allows us to express the reaction constant in terms of the Gibbs free energy of activation $\Delta_A G$

$$\mathfrak{K} = A' \exp\left(\frac{-\Delta_A H - T\Delta_A S}{RT}\right) = A' \exp\left(\frac{-\Delta_A G}{RT}\right) \tag{32}$$

Advanced kinetic theories (e.g., transition state theory) have tried to estimate the values of A and $\Delta_A E$ corresponding to a certain electrochemical reaction and to relate them to molecular properties. However, extending our discussion to such complex descriptions is outside the scope of this work. For the interested reader, a deeper discussion of electron transfer kinetics can be found in Ref. [90].

[3] A detailed description of the development of Arrhenius equation is presented by [88]. An English translation of the original paper of Arrhenius can be found in Ref. [89], first edited in 1967, pp. 31–35.

[4] In general $\Delta H = \Delta E + \Delta(pV)$ but in condensed-phase reactions $\Delta(pV)$ can be neglected, so that $\Delta E \approx \Delta H$ [90].

5.1.1. Single-step single-electron reactions

To fix ideas, let us consider a generic single-step reversible electrooxidation reaction (similar to the anode half-reaction of a PEMFC) involving the transfer of a single electron

$$\mathrm{R} \rightleftharpoons \mathrm{O} + e^{-} \tag{33}$$

At this point, it is important to note that the Gibbs free energy of activation at a given condition can be written as the Gibbs free energy of activation at a reference state, usually taken as the equilibrium state, hereafter denoted by the subscript 0, plus an additional term that accounts for the deviation of the potential from its value at the reference state. Thus, for the forward (i.e., oxidation) reaction

$$\Delta_A G_{\mathrm{O}x} = \Delta_A G^0 - \alpha_{\mathrm{O}x} F\left(E - E^0\right) \tag{34}$$

while for the backward (i.e., reduction) reaction

$$\Delta_A G_{\mathrm{Red}} = \Delta_A G^0 + \alpha_{\mathrm{Red}} F\left(E - E^0\right) \tag{35}$$

where $\alpha_{\mathrm{O}x}$ and $\alpha_{\mathrm{R}ed}$ are the charge transfer coefficients of the oxidation and reduction reactions. The charge transfer coefficients reflect the nature of the electron transfer process in single-step electrochemical reactions [86]. For single electron reactions taking place on metallic surfaces, the value $\alpha_{\mathrm{O}x} \approx 0.5$ is commonly accepted [11, 91]. The value of $\alpha_{\mathrm{O}x}$ is also related to the charge transfer coefficient of the backward reaction, with the symmetry relation $\alpha_{\mathrm{R}ed} = 1 - \alpha_{\mathrm{O}x}$ being frequently assumed. For a thorough derivation of the above expressions, the reader is referred to Section 3.3.2 of the book of Bard and Faulkner [90].

According to Eqs. (32), (34), and (35), the reaction constants for the forward and backward reactions can be written as

$$\begin{aligned} \mathfrak{K}_{\mathrm{O}x} &= A'_{\mathrm{Ox}} \exp\left(\frac{-\Delta_A G_{\mathrm{O}x}}{RT}\right) = A'_{\mathrm{Ox}} \exp\left(\frac{-\Delta_A G^0_{\mathrm{O}x}}{RT}\right) \exp\left(\alpha_{\mathrm{Ox}} \frac{F\left(E - E^0\right)}{RT}\right) \\ \mathfrak{K}_{\mathrm{Red}} &= A'_{\mathrm{Red}} \exp\left(\frac{-\Delta_A G_{\mathrm{R}ed}}{RT}\right) = A'_{\mathrm{Red}} \exp\left(\frac{-\Delta_A G^0_{\mathrm{R}ed}}{RT}\right) \exp\left(-\alpha_{\mathrm{Red}} \frac{F\left(E - E^0\right)}{RT}\right) \end{aligned} \tag{36}$$

When expressed in moles of species R consumed per unit catalyst surface per unit time, the net reaction rate can be written as follows

$$\Gamma = C_{\mathrm{R}} K_{\mathrm{Ox}} \exp\left(\alpha_{\mathrm{Ox}} \frac{F\left(E - E^0\right)}{RT}\right) - C_{\mathrm{O}} K_{\mathrm{Red}} \exp\left(-\alpha_{\mathrm{Red}} \frac{F\left(E - E^0\right)}{RT}\right) \tag{37}$$

where the constants $K_{\mathrm{O}x}$ and $K_{\mathrm{R}ed}$ incorporate all the terms that are independent of the potential

$$K_r = A'_r \exp\left(\frac{-\Delta_A G^0_r}{RT}\right), \quad r = \mathrm{O}x, \ \mathrm{Red} \tag{38}$$

In general, the reaction constants K_r appearing in Eq. (37) depend on the temperature T, the reaction being studied, and the type of catalyst where the reaction takes place.

To continue the discussion, it is convenient now to consider the equilibrium condition. At equilibrium, the net reaction rate Γ is zero, since oxidation and reduction occur at the same rate. At this state, the potential reaches an equilibrium value, $E^\star$, and the same happens with the concentrations, $C_R^\star$ and $C_O^\star$. From Eq. (37), at equilibrium, the reaction rate of the oxidation and reduction reactions can be written as

$$\Gamma^\star = C_R^\star K_{Ox} \exp\left(\frac{\alpha_{Ox} F\left(E^\star - E^0\right)}{RT}\right) = C_O^\star K_{Red} \exp\left(-\frac{\alpha_{Red} F\left(E^\star - E^0\right)}{RT}\right) \tag{39}$$

Dividing Eq. (37) by $\Gamma^\star$ and rearranging yields

$$\frac{\Gamma}{\Gamma^\star} = \frac{C_R}{C_R^\star} \exp\left(\frac{\alpha_{Ox} F\left(E - E^\star\right)}{RT}\right) - \frac{C_O}{C_O^\star} \exp\left(\frac{-\alpha_{Red} F\left(E - E^\star\right)}{RT}\right) \tag{40}$$

This expression for Γ circumvents the difficulty of referring the potential to the standard potential, as the overpotential is much simpler to measure experimentally. It was Tafel [85] the first to write the reaction rate in this form, which can also be expressed as

$$\Gamma = \Gamma^\star \left[\frac{C_R}{C_R^\star} \exp\left(\frac{\alpha_{Ox} F\eta}{RT}\right) - \frac{C_O}{C_O^\star} \exp\left(\frac{-\alpha_{Red} F\eta}{RT}\right)\right] \tag{41}$$

in terms of the overpotential, $\eta = E - E^\star$. This equation is very often written using the simpler notation

$$\Gamma = C_R k_{Ox} \exp\left(\frac{\alpha_{Ox} F\eta}{RT}\right) - C_O k_{Red} \exp\left(\frac{-\alpha_{Red} F\eta}{RT}\right) \tag{42}$$

in terms of the oxidation and reduction rate constants

$$k_{Ox} = \frac{\Gamma^\star}{C_R^\star} \quad \text{and} \quad k_{Red} = \frac{\Gamma^\star}{C_O^\star} \tag{43}$$

The net current density generated by the electrochemical redox reaction, expressed in amperes per unit catalyst surface area, can be obtained by multiplying the net reaction rate Γ given in (41) by Faraday's constant, resulting in the well-known *Butler-Volmer equation*

$$j = j_0 \left[\frac{C_R}{C_R^\star} \exp\left(\frac{\alpha_{Ox} F\eta}{RT}\right) - \frac{C_O}{C_O^\star} \exp\left(\frac{-\alpha_{Red} F\eta}{RT}\right)\right] \tag{44}$$

where $j_0 = \Gamma^\star F$ is the so-called *exchange current density*, a fundamental electrochemical property that represents the rate of the oxidation and reduction reactions at equilibrium expressed in terms of current density. It is interesting to note that Butler [92] and Volmer [93] found this equation separately, so the name honors both. Under conditions where the backward reaction

can be neglected, for example, for sufficiently high overpotentials, Eq. (44) reduces to the *Tafel equation*, which is written here in exponential form

$$j = FC_R k_{Ox} \exp\left(\frac{\alpha_{Ox} F\eta}{RT}\right) \quad \text{or} \quad \eta = \frac{RT}{\alpha_{Ox}F}\ln j - \frac{RT}{\alpha_{Ox}F}\ln\left(FC_R k_{Ox}\right) \tag{45}$$

It should be noted that the original *Tafel equation* was written using the decimal logarithm, which yields the factor 2.3 in Eq. (29).[5]

The current density, j, appearing in Eqs. (29), (44), and (45) requires further comment. This current density is expressed in amperes per unit catalyst surface area. In order to convert it to amperes per unit volume, as often required for evaluating distributed current sources in three-dimensional macro-homogeneous models of fuel cell catalysts layers, the current density j has to be multiplied by a geometric factor representing the catalyst surface area per unit volume of catalyst layer. This conversion factor is the so-called *volume-specific catalyst surface area*, often denoted by the letter a in the literature. Integrating the volumetric current density aj over the thickness of the catalyst layer at a certain location, one obtains the cell current density, hereafter denoted by i, which represents the current generated by the cell per unit surface area of catalyst layer and coincides with the protonic current density crossing the membrane.

5.1.2. Multiple-step multiple-electron reactions

Electrochemical reactions in fuel cells usually involve more than a single step and more than a single electron transfer. To deal with multistep reactions involving the transfer of several electrons, it is convenient to assume that there exists an elementary step that is significantly slower than the rest, the so-called *rate-determining step* (RDS) of the global reaction. Some authors [11, 94] propose the relation

$$\alpha_{Ox} + \alpha_{Red} = \frac{n}{\upsilon} \tag{46}$$

where n is the total number of electrons transferred and υ is the number of times that the RDS must occur for the overall reaction to occur. Other authors [86] propose to write the charge transfer coefficient as a function of the overpotential following *Marcus theory*

$$\alpha_{Ox} = \frac{1}{2}\left(1 + \frac{F\eta}{\lambda}\right) \tag{47}$$

where the parameter λ is referred to as the *reorganization energy*, defined as the energy required to change the nuclear configurations [95][6].

[5] $\ln x = \log x / \log e \approx 2.3 \log x$.

[6] Rudolph A. Markus received the 1992 Nobel Prize in Chemistry "for his contributions to the theory of electron transfer reactions in chemical systems". An extended review of Markus theory is presented in his review [96]. An extension to organic reactions is presented in Ref. [97].

http://dx.doi.org/10.5772/intechopen.71635

Nevertheless, a closer look at the reactions involved in the whole process will give us a better understanding. For a general electrochemical reaction of the form

$$\mathrm{R} \rightleftharpoons \mathrm{O} + ne^- \tag{48}$$

the reaction mechanism could be divided in three parts: the reactions before the RDS

$$\mathrm{R} \rightleftharpoons \mathrm{R}' + n'e^- \tag{49}$$

the RDS itself

$$\mathrm{R}' \rightleftharpoons \mathrm{O}' + e^- \tag{50}$$

and the reactions after the RDS

$$\mathrm{O}' \rightleftharpoons \mathrm{O} + n''e^- \tag{51}$$

As the RDS acts effectively as a bottleneck for the multistep reaction process, the reaction rate of the global reaction is given in first approximation by that of the RDS. Applying Eq. (42) to the RDS, the following expression is obtained

$$\Gamma = C_{\mathrm{R}'} k_{\mathrm{Ox}}^{\mathrm{RDS}} \exp\left(\frac{\alpha_{\mathrm{Ox}}^{\mathrm{RDS}} F\left(E - E^{\star RDS}\right)}{RT}\right) - C_{\mathrm{O}'} k_{\mathrm{Red}}^{\mathrm{RDS}} \exp\left(\frac{-\alpha_{\mathrm{Red}}^{\mathrm{RDS}} F\left(E - E^{\star \mathrm{RDS}}\right)}{RT}\right) \tag{52}$$

Pre- and post-RDS reactions take place significantly faster than the RDS. As a result, the concentration of the intermediate compounds (namely R′ and O′) can be approximated by the equilibrium values obtained from the pre- and post-RDS reactions, respectively. Combining Eq. (42) and the equilibrium condition ($\Gamma = 0$) applied to the pre- and post-RDS reactions, expressions for the concentration of the intermediate compounds in terms of the initial and final products (R and O) can be obtained

$$\begin{aligned} C_{\mathrm{R}'} &= C_{\mathrm{R}} \frac{k'_{\mathrm{Ox}}}{k'_{\mathrm{Red}}} \exp\left(\frac{\left(\alpha'_{\mathrm{Ox}} + \alpha'_{\mathrm{Red}}\right) F\left(E - E'^{\star}\right)}{RT}\right) \\ C_{\mathrm{O}'} &= C_{\mathrm{O}} \frac{k''_{\mathrm{Red}}}{k''_{\mathrm{Ox}}} \exp\left(\frac{-\left(\alpha''_{\mathrm{Ox}} + \alpha''_{\mathrm{Red}}\right) F\left(E - E''^{\star}\right)}{RT}\right) \end{aligned} \tag{53}$$

Substituting these expressions in Eq. (52) yields the following expression for the reaction rate of the multistep electrochemical reaction

$$\begin{aligned} \Gamma = C_{\mathrm{R}} \frac{k_{\mathrm{Ox}}^{\mathrm{RDS}} k'_{Ox}}{k'_{\mathrm{Red}}} \exp\left(\left[-\left(\alpha'_{\mathrm{Ox}} + \alpha'_{\mathrm{Red}}\right) E'^{\star} + \alpha^{\mathrm{RDS}} E^{\mathrm{RDS}\star}\right] \frac{F}{RT}\right) \\ \times \exp\left(\left(\alpha'_{\mathrm{Ox}} + \alpha'_{\mathrm{Red}} + \alpha_{\mathrm{Ox}}^{\mathrm{RDS}}\right) E \frac{F}{RT}\right) - \end{aligned}$$

$$C_O \frac{k_{Red}^{RDS} k'_{Red}}{k'_{Ox}} \exp\left(\left[(\alpha''_{Ox} + \alpha''_{Red})E''^{\star} - \beta^{RDS} E^{RDS\star}\right]\frac{F}{RT}\right)$$
$$\times \exp\left(-(\alpha''_{Ox} + \alpha''_{Red} + \alpha_{Red}^{RDS})E\frac{F}{RT}\right) \tag{54}$$

The above expression involves absolute potentials, which can not be readily measured. In order to express the overall reaction rate Γ in a more convenient way, the first and second terms can be multiplied by the unit factors

$$\exp\left((\alpha'_{Ox} + \alpha'_{Red} + \alpha_{Ox}^{RDS})\frac{F(E^{\star} - E^{\star})}{RT}\right)$$
$$\text{and} \quad \exp\left((\alpha''_{Ox} + \alpha''_{Red} + \alpha_{Red}^{RDS})\frac{F(E^{\star} - E^{\star})}{RT}\right) \tag{55}$$

where $E^{\star}$ denotes the equilibrium potential of the complete reaction. This results in the following expression

$$\Gamma = C_R \overbrace{\frac{k_{Ox}^{RDS} k'_{Ox}}{k'_{Red}} \exp\left(\left[-(\alpha'_{Ox} + \alpha'_{Red})\left(E'^{\star} - E^{\star}\right) + \alpha_{Ox}^{RDS}\left(E^{RDS\star} - E^{\star}\right)\right]\frac{F}{RT}\right)}^{k_{Ox}}$$
$$\times \exp\left(\overbrace{(\alpha'_{Ox} + \alpha'_{Red} + \alpha_{Ox}^{RDS})}^{\alpha_{Ox}}\frac{F(E - E^{\star})}{RT}\right)$$
$$- C_O \underbrace{\frac{k_{Red}^{RDS} k''_{Red}}{k''_{Ox}} \exp\left(\left[(\alpha''_{Ox} + \alpha''_{Red})\left(E''^{\star} - E^{\star}\right) + \alpha_{Red}^{RDS}\left(E^{RDS\star} - E^{\star}\right)\right]\frac{F}{RT}\right)}_{k_{Red}} \tag{56}$$
$$\times \exp\left(-\underbrace{(\alpha''_{Ox} + \alpha''_{Red} + \alpha_{Red}^{RDS})}_{\alpha_{Red}}\frac{F(E - E^{\star})}{RT}\right)$$

which can be rewritten as Eq. (42) by introducing the overpotential η to give

$$\Gamma = C_R k_{Ox} \exp\left(\frac{\alpha_{Ox} F\eta}{RT}\right) - C_O k_{Red} \exp\left(-\frac{\alpha_{Red} F\eta}{RT}\right) \tag{57}$$

The above discussion demonstrates how is it possible to define global charge transfer coefficients, α_{Ox} and α_{Red}, and rate constants, k_{Ox} and k_{Red}, for the overall electrochemical reaction from those of the elementary reaction steps. This technique provides a powerful tool for the analysis of complex electrochemical systems, such as the multistep ethanol oxidation reaction (EOR) to be discussed below. As will be seen, the introduction of global kinetic parameters for certain reaction paths is particularly useful when trying to adjust the kinetic constants so as to fit the selectivities of the final products.

5.2. Coverage factors

The electrochemical reactions that take place in a fuel cell need not only to occur but also to have a sufficiently high reaction rate. To provide a favorable environment for the reactions, catalysts are always used in fuel cells. A catalyst is a compound that favors the chemical reaction, but it is not involved in it. The catalyst acts as substrate for the reaction, in that its surface has *places* where the fuel molecules *take place* to proceed with the reaction. In fuel cells, catalysts are pinned up to a porous matrix. The process where the reactive molecules *take place* at the catalyst sites is called adsorption. Once the molecules have been adsorbed, they no longer behave as free molecules; they remain attached to the catalyst site. The so-called adsorbates may undergo electrochemical reaction and later be desorbed as reaction products or, alternatively, be desorbed as unreacted free molecules.

The catalyst acts as an anchor to the adsorbed species. The concentration of these species has no physical meaning because they fill spaces where there are catalyst places; actually, they *cover* the catalyst surface. This behavior is equivalent to the adsorption described by [98] for the atomic deposition over glass surfaces. The amount of absorbed species is thus described by the *surface coverage factor*, Θ, which represents the fraction of the catalyst sites occupied by this species.

The coverage factor of a given species cannot be larger than unity (full coverage of the catalyst places). And if different species can be adsorbed into the same catalyst type, the sum of their coverage factors cannot exceed unity either

$$\sum_k \Theta_k \leq 1 \tag{58}$$

From the definition of the coverage factors, the fraction of free catalyst sites is given by

$$\Theta_{\mathrm{F}} = 1 - \sum_k \Theta_k \tag{59}$$

Using these expressions, it is possible to evaluate the net adsorption rate of species k. The adsorption rate is proportional to the available catalyst sites, while the desorption rate is proportional to the fraction of occupied sites, so that

$$q_k = \mathfrak{K}_{\mathrm{ads}}\Theta_{\mathrm{F}} - \mathfrak{K}_{\mathrm{des}}\Theta_k \tag{60}$$

where the proportionality constants $\mathfrak{K}_{ads}$ and $\mathfrak{K}_{des}$ depend on the kind of absorption mechanism. Langmuir [98] applied this model to the adsorption of a monoatomic layer in a flat surface (e.g., glass); in electrochemical reactions, the absorption/desorption processes often involve reactions with charge transfer. In these cases, the adsorbed species is not the same as the free specie, but Eq. (60) can still be used with the required modifications.

As previously discussed, the reaction rates of the forward and backward reactions are proportional to the molar concentrations of reactants and products, respectively. When an adsorbed species is involved, its concentration is equal to the coverage factor of the adsorbate times the concentration C_c of the catalyst

$$C_k = \Theta_k C_c \tag{61}$$

where C_c remains unchanged during the reaction. As a result, for adsorption/desorption reactions, the catalyst concentration is usually included in the reaction constants, which are thus also strongly affected by the catalysts type. The use of coverage factors in kinetic models of catalytic reactions is widely used in fuel cell modeling [77, 99–104], and will be illustrated in the example presented below.

6. Modeling the ethanol electro-oxidation reaction

Ethanol offers an interesting alternative as a fuel for PEM fuel cells because it can be readily produced by fermentation of biomass, including agricultural raw materials, which makes it currently the major renewable biofuel. On top of that, its mass energy density is about 30% larger than that of methanol, and it is much less toxic [27, 64]. However, the electrooxidation of the complex ethanol molecule is much slower than that of methanol. The ethanol oxidation reaction (EOR) is known to proceed through a multistep reaction process that involves adsorbed species like acetyl (CH_3CO_{ads}) and carbon monoxide (CO_{ads}), leading to a variety of partial oxidation products such as acetaldehyde (CH_3CHO), acetic acid (CH_3COOH), carbon dioxide (CO_2), and methane (CH_4).

6.1. The ethanol oxidation reaction

According to the above discussion, one of the main difficulties encountered in the modeling of DEFCs is the accurate description of the EOR. Different reaction mechanisms have been proposed in the literature [38, 44, 45, 50, 106]. Due to the large amount of intermediate species, both free and adsorbed, and of potential elementary reactions, mathematical models exhibit different levels of complexity [77, 107, 108]. As a particular example, **Figure 2** shows a reaction mechanism for the EOR on binary Pt-based catalysts recently proposed by the authors [105], based on a previous model by Meyer et al. [77] which ignored Reactions I, II, and III. The kinetic model assumes that there are eleven elementary reactions, listed in **Table 2**, involving five adsorbed species, four of them attached to the Pt-sites (CH_3CHOH_{ads}, CH_3CO_{ads}, CO_{ads} and $CH_{3\,ads}$), and the fifth (OH_{ads}) to the secondary metal following the bifunctional catalyst assumption [53–55].

The full derivation of the model can be found elsewhere [105]. Here we will only consider Reactions I and III to illustrate the application of the electrochemical rate laws introduced in the previous sections. Reaction I represents the adsorption of ethanol to CH_3CHOH_{ads}. This is an oxidative adsorption reaction, with a net adsorption rate (in moles per unit volume of catalyst layer per unit time) given by

$$\begin{aligned} q_{\mathrm{I}} = {} & \left(1 - \Theta_{CH_3CHOH_{ads}} - \Theta_{CH_3CO_{ads}} - \Theta_{CO_{ads}} - \Theta_{CH_{3\,ads}}\right) C_{\mathrm{E,\,acl}} k_{\mathrm{If}} \exp\left(\frac{\alpha_{\mathrm{I}} F}{RT}\eta_a\right) \\ & - \Theta_{CH_3CHOH_{ads}} k_{\mathrm{Ib}} \exp\left(-\frac{(1-\alpha_{\mathrm{I}})F}{RT}\eta_a\right) \end{aligned} \tag{62}$$

http://dx.doi.org/10.5772/intechopen.71635

The factor between brackets appearing in the forward reaction rate gives the fraction of available Pt-sites, reduced due to the presence of the adsorbates, which act as site-blocker. Note that this term does not account for the presence of adsorbed OH groups, because in the binary catalysts typically used in DEFCs they are preferably attached to the secondary metal. Reaction 3 represents the dissociative adsorption of water to yield adsorbed hydroxyl groups, a reaction that in binary Pt-based catalysts occurs on the secondary metal. The resulting water activation rate is given by

$$q_3 = k_{3f}\left(1-\Theta_{OH_{ads}}\right)\exp\left(\frac{\alpha_3 F}{RT}\eta_a\right) - k_{3b}\Theta_{OH_{ads}}\exp\left(-\frac{(1-\alpha_3)F}{RT}\eta_a\right) \tag{63}$$

where now the forward reaction rate is proportional to the fraction of free sites existing on the secondary catalyst, only blocked by the adsorbed hydroxyl groups, while the inverse reaction is proportional to the coverage factor of this adsorbate. In these expressions, α_i are the global charge transfer coefficients and k_i the global reaction constants, which could be related to those of the elementary reaction steps involved in each global reaction as suggested in Eqs. (56) and (57). It

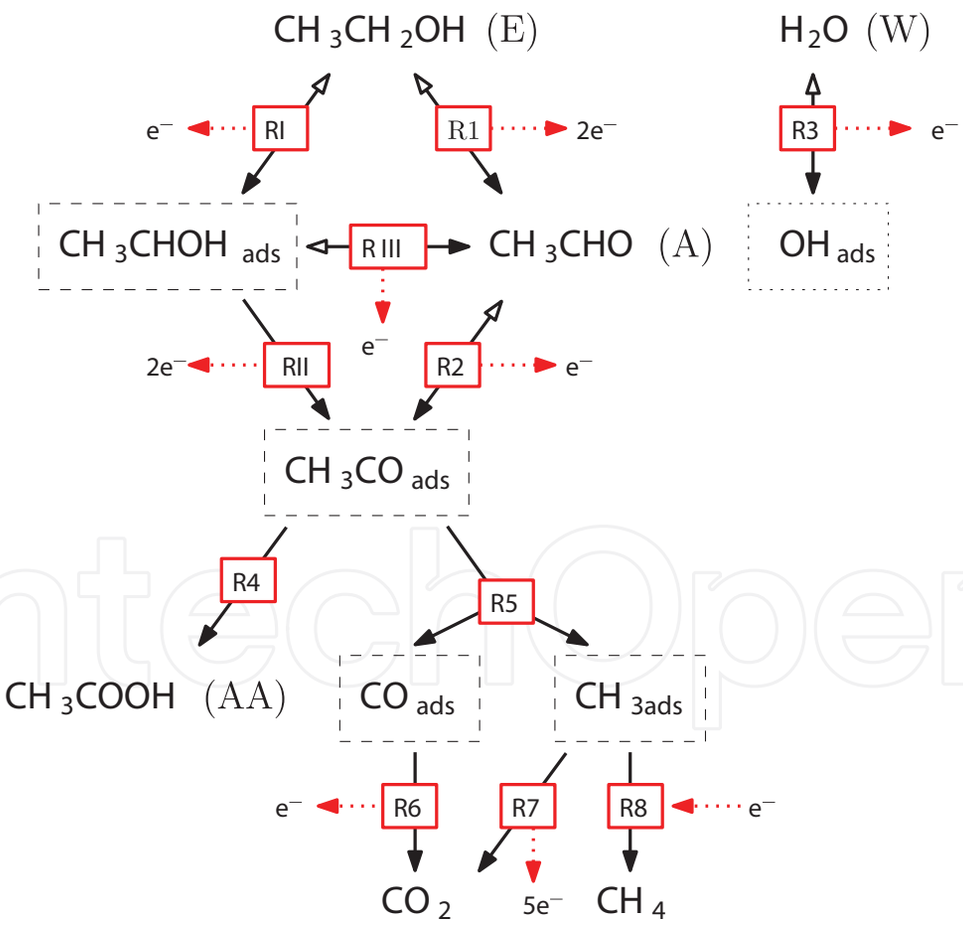

Figure 2. Reaction mechanism for the electron oxidation reaction (EOR) on binary Pt-based catalysts proposed in Ref. [105]. Pt-site adsorbed species are indicated by a dashed box; OH_{ads} is boxed using dotted lines to indicate that it is adsorbed at the secondary metal sites. Reactions 4, 6, and 7 use the adsorbed hydroxyl groups to proceed. The exact stoichiometries are shown in **Table 2**.

should be noted that the volume-specific molar reaction rates, q_r, can be readily obtained from the surface-specific molar reaction rates, Γ_r, discussed in Section 5 by multiplying the latter by the volume-specific catalyst surface area, $q_r = a\Gamma_r$.

Similar rate laws can be written for the remaining reaction steps, leading to a full kinetic model that involves 26 adjustable kinetic parameters: 9 transfer coefficients and 17 reaction constants (see **Table 2**). Using the quasi-steady-state approximation for the adsorbates, that is, assuming that the coverage factors θ_k do not change with time, yields a nonlinear system of equations that can be solved to evaluate the θ_k in terms of the local conditions at the anode catalyst layer. Complementing the kinetic model with appropriate descriptions for mass and charge transport gives rise to a suitable mathematical model for the anode of a DEFC. This model provides, in particular, polarization and power density curves, as well as the variation of the product selectivity and effective electron generation number as a function of the local current density. Using anode polarization and product selectivity data obtained from carefully designed experiments [75], the kinetic parameters can be fitted to reproduce the observed results, leading to a fully predictive model of the anode of a DEFC [105].

6.2. The oxygen reduction reaction

Although the oxygen reduction reaction (ORR) is much simpler than the EOR, it is also known to be a multistep reaction, involving the formation of a number of intermediate

Reaction	—	—	n_α
I. $CH_3CH_2OH \rightleftharpoons CH_3CHOH_{ads} + H^+ + e^-$	k_{If}	α_I	1
	k_{Ib}	—	1
II. $CH_3CHOH_{ads} \rightarrow CH_3CO_{ads} + 2H^+ + 2e^-$	k_{IIf}	α_{II}	2
	k_{IIb}	—	2
III. $CH_3CHOH_{ads} \rightleftharpoons CH_3CHO + H^+ + e^-$	k_{IIIf}	α_{III}	1
	k_{IIIb}	—	1
1. $CH_3CH_2OH \rightleftharpoons CH_3CHO + 2H^+ + 2e^-$	k_{1f}	α_1	2
	k_{1b}	—	2
2. $CH_3CHO \rightleftharpoons CH_3CO_{ads} + H^+ + e^-$	k_{2f}	α_2	1
	k_{2b}	—	1
3. $H_2O \rightleftharpoons OH_{ads} + H^+ + e^-$	k_{3f}	α_3	1
	k_{3b}	—	1
4. $CH_3CO_{ads} + OH_{ads} \rightarrow CH_3COOH$	k_4	—	—
5. $CH_3CO_{ads} \rightarrow CO_{ads} + CH_{3\,ads}$	k_5	—	—
6. $CO_{ads} + OH_{ads} \rightarrow CO_2 + H^+ + e^-$	k_6	α_6	1
7. $CH_{3\,ads} + 2OH_{ads} \rightarrow CO_2 + 5H^+ + 5e^-$	k_7	α_7	5
8. $CH_{3\,ads} + H^+ + e^- \rightarrow CH_4$	k_8	α_8	1

Table 2. The 11-step reaction mechanism proposed in [105].

species. The complex nature of the ORR is reflected by the doubling of the Tafel slope at intermediate potentials, which is thought to occur due to a change in the rate determining step of the reaction [78]. This change can be qualitatively described using the double-trap kinetic model [109], which involves four elementary reaction steps: dissociative adsorption of O_2 to O_{ads}, reductive adsorption of O_2 to OH_{ads}, reductive transition of O_{ads} to OH_{ads}, and reductive desorption of OH_{ads} to H_2O. However, reproducing quantitatively the doubling of the Tafel slope requires a more detailed analysis, similar to the one discussed above for the EOR. Complementing the kinetic rate expressions for the four elementary steps with the quasi-steady-state approximation for the two adsorbates, O_{ads} and OH_{ads}, and using appropriate experimental data in order to fit a certain set of adjustable parameters using optimization algorithms, a fully predictive ORR kinetic model is finally obtained [110].

However, the kinetic model of the ORR proposed in Ref. [110] is anticipated to fail when applied to the cathode of a DEFC. In this case, the effect of the parasitic reactions induced by ethanol and acetaldehyde crossover is expected to affect the reaction kinetics in two ways: (1) by introducing mixed potentials required to draw the excess (i.e., parasitic) current density due to crossover and (2) by poisoning the catalyst by adsorbed intermediates of the parasitic reactions, which block a large amount of the available active catalyst sites [111]. Further research is still needed to clarify these complex electrochemical phenomena, which will surely benefit from the systematic approach laid out by the recent investigations discussed in this chapter.

7. Conclusions

In this chapter, the thermodynamic and electrochemical principles of PEM fuel cells have been presented and discussed. These principles have been applied to the study of a complex electrochemical system, the direct ethanol fuel cell, reviewing recent work on this problem and suggesting future research directions.

Nomenclature

Symbols

a_k Activity of species k

C_k Molar concentration of species k [mol m^{-3}]

E Electric potential [V]

F Faraday constant $F = 96480$ C

h Molar enthalpy [J mol^{-1}]

H Enthalpy [J]

g Molar Gibbs free energy [J mol^{-1}]

G Gibbs free energy [J]

I Electric current [A]

i Electric current density [A m^{-2}]

j Electric current density per catalyst surface area [A m^{-2}]

n Number of electrons transferred

N_k Molar flux of species k [mol m^{-2} s^{-1}]

p_k Pressure of species k [Pa]

Q Heat [W]

q Volume-specific molar rate of reaction [mol m^3 s^{-1}]

R Ideal-gas constant 8.3143 [J mol^{-1} K^{-1}]

s Molar entropy [J K^{-1} mol^{-1}]

S Entropy [J K^{-1}]

T Temperature [K]

V Electric voltage [V]

W_e Electrical work [W]

Greek letters

α Charge transfer coefficient

Γ Surface-specific molar rate of reaction [mol m^2 s^{-1}]

η Overpotential $\eta = E - E^{\star}$ [V]

Θ_k Coverage factor of species k

μ_k Chemical potential of species k

ρ Density [kg m^3]

v_k Stoichiometric coefficient species k [0.35 cm]

ac/agdl Anode channel/gdl interface

cc/cgdl Cathode channel/gdl interface

e Electric

f Formation

k Species

Ox Oxidation reaction

r	Reaction
Red	Reduction reaction

Superscripts

0	Reference state conditions
⋆	Equilibrium state conditions

Author details

Juan Sánchez-Monreal, Marcos Vera* and Pablo A. García-Salaberri

*Address all correspondence to: marcos.vera@uc3m.es

Dept. de Ingeniería Térmica y de Fluidos, Escuela Politécnica Superior, Universidad Carlos III de Madrid, Leganés, Spain

References

[1] Grove WR. On voltaic series and the combination of gases by platinum. Philosophical Magazine: Series 3. 1839;**14**(86–87):127-130

[2] Grove WR. On a gaseous voltaic battery. Philosophical Magazine: Series 3. 1842;**21** (140):417-420

[3] Bossel U. The Birth of the Fuel Cell, 1835–1845: Including the First Publication of the Complete Correspondence from 1839 to 1868 between Christian Friedrich Schoenbein (discoverer of the Fuel Cell Effect) and William Robert Grove (inventor of the Fuel Cell). European Fuel Cell Forum. 2000

[4] Appleby AJ. From Sir William Grove to today: Fuel cells and the future. Journal of Power Sources. 1990;**29**(1–2):3-11

[5] Perry ML, Fuller TF. A historical perspective of fuel cell technology in the 20th century. Journal of the Electrochemical Society. 2002;**149**(7):s59-s67

[6] U.S. DOE. The Fuel Cells Technologies Office Multi-Year Research, Development, and Demonstration Plan. Technical report: U.S. Department of Energy; 2016

[7] Wang Y, Chen KS, Mishler J, Cho SC, Adroher XC. A review of polymer electrolyte membrane fuel cells: Technology, applications, and needs on fundamental research. Applied Energy. 2011;**88**(4):981-1007

[8] Cipriani G, Di Dio V, Genduso F, La Cascia D, Liga R, Miceli R, Ricco Galluzzo G. Perspective on hydrogen energy carrier and its automotive applications. International Journal of Hydrogen Energy. 2014;**39**(16):8482-8494

[9] Jiao K, Li X. Water transport in polymer electrolyte membrane fuel cells. Progress in Energy and Combustion Science. 2011;**37**(3):221-291

[10] Jiao K. Experimental and Modelling Studies of Cold Start Processes in Proton Exchange Membrane Fuel Cells. PhD Thesis. UWSpace. 2001. http://hdl.handle.net/10012/6010

[11] Barbir F. PEM Fuel Cells: Theory and Practice. Elsevier Academic. 2005

[12] O'Hayre R, Fabian T, Litster S, Prinz FB, Santiago JG. Engineering model of a passive planar air breathing fuel cell cathode. Journal of Power Sources. 2007;**167**(1):118-129

[13] Kelley RJ, Pratt SD, Landreth BD, Pennisi RW, Muthuswamy S, Urbish GF. Portable Fuel Cell Power Supply. U.S. Patent No. 6,268,077. Washington, DC: U.S. Patent and Trademark Office. 2001

[14] Guo Z, Cao Y. A passive fuel delivery system for portable direct methanol fuel cells. Journal of Power Sources. 2004;**132**(1):86-91

[15] Chu D, Jiang R. Performance of polymer electrolyte membrane fuel cell (PEMFC) stacks. Journal of Power Sources. 1999;**83**(1–2):128-133

[16] Fabian T, Posner JD, O'Hayre R, Cha S-W, Eaton JK, Prinz FB, Santiago JG. The role of ambient conditions on the performance of a planar, air-breathing hydrogen PEM fuel cell. Journal of Power Sources. 2006;**161**(1):168-182

[17] Chen CY and Yang P. Performance of an Air-Breathing Direct Methanol Fuel Cell. Journal of Power Sources. 2003;**123**(1);37-42

[18] Pereira JP, Falcão DS, Oliveira VB, Pinto AMFR. Performance of a passive direct ethanol fuel cell. Journal of Power Sources. 2014;**256**:14-19

[19] Kamarudin SK, Achmad F, Daud WRW. Overview on the application of direct methanol fuel cell (DMFC) for portable electronic devices. International Journal of Hydrogen Energy. 2009;**34**(16):6902-6916

[20] Logan BE, Hamelers B, Rozendal R, Schröder U, Keller J, Freguia S, Aelterman P, Verstraete W, Rabaey K. Microbial fuel cells: Methodology and technology. Environmental Science & Technology. 2006;**40**(17):5181-5192

[21] Yang C, Costamagna P, Srinivasan S, Benziger J, Bocarsly AB. Approaches and technical challenges to high temperature operation of proton exchange membrane fuel cells. Journal of Power Sources. 2001;**103**(1):1-9

[22] Chandan A, Hattenberger M, El-kharouf A, Du S, Dhir A, Self V, Pollet BG, Ingram A, Bujalski W. High temperature (HT) polymer electrolyte membrane fuel cells (PEMFC) – A review. Journal of Power Sources. 2013;**231**:264-278

[23] Lamy C, Lima A, LeRhun V, Delime F, Coutanceau C, Lèger J-M. Recent advances in the development of direct alcohol fuel cells (DAFC). Journal of Power Sources. 2002; **105**(2):283-296

[24] Lamy C, Belgsir EM, Lèger J-M. Electrocatalytic oxidation of aliphatic alcohols: Application to the direct alcohol fuel cell (DAFC). Journal of Applied Electrochemistry. 2001;**31**(7): 799-809

[25] Lamy C, Rousseau S, Belgsir EM, Coutanceau C, Lèger J-M. Recent progress in the direct ethanol fuel cell: Development of new platinum—tin electrocatalysts. Electrochimica Acta. 2004;**49**(22–23):3901-3908

[26] Soloveichik GL. Liquid fuel cells. Beilstein Journal of Nanotechnology. 2014;**5**(1):1399-1418

[27] Kamarudin MZF, Kamarudin SK, Masdar MS, Daud WRW. Review: Direct ethanol fuel cells. International Journal of Hydrogen Energy. 2013;**38**(22):9438-9453

[28] Horacio R. Corti and Ernesto R. Gonzalez, Editors. Direct Alcohol Fuel Cells. Netherlands, Dordrecht: Springer; 2014

[29] Nacef M, Affoune AM. Comparison between direct small molecular weight alcohols fuel cells' and hydrogen fuel cell's parameters at low and high temperature. Thermodynamic study. International Journal of Hydrogen Energy. 2011;**36**(6):4208-4219

[30] Heinzel A, Barragán VM. A review of the state-of-the-art of the methanol crossover in direct methanol fuel cells. Journal of Power Sources. 1999;**84**(1):70-74

[31] Ravikumar MK, Shukla AK. Effect of methanol crossover in a liquid-feed polymer-electrolyte direct methanol fuel cell. Journal of the Electrochemical Society. 1996;**143**(8):2601

[32] Gurau B, Smotkin ES. Methanol crossover in direct methanol fuel cells: A link between power and energy density. Journal of Power Sources. 2002;**112**(2):339-352

[33] James DD, Pickup PG. Effects of crossover on product yields measured for direct ethanol fuel cells. Electrochimica Acta. 2010;**55**(11):3824-3829

[34] Song S, Wang G, Zhou W, Zhao X, Sun G, Xin Q, Kontou S, Tsiakaras P. The effect of the MEA preparation procedure on both ethanol crossover and DEFC performance. Journal of Power Sources. 2005;**140**(1):103-110

[35] Andreadis GM, Tsiakaras PE. Ethanol crossover and direct ethanol PEM fuel cell performance modeling and experimental validation. Chemical Engineering Science. 2006; **61**(22):7497-7508

[36] Song S, Zhou W, Tian J, Cai R, Sun G, Xin Q, Kontou S, Tsiakaras P. Ethanol crossover phenomena and its influence on the performance of DEFC. Journal of Power Sources. 2005;**145**(2):266-271

[37] Andreadis GM, Podias AKM, Tsiakaras PE. The effect of the parasitic current on the direct ethanol PEM fuel cell operation. Journal of Power Sources. 2008;**181**(2):214-227

[38] Kutz RB, Braunschweig B, Mukherjee P, Behrens RL, Dlott DD, Wieckowski A. Reaction pathways of ethanol electrooxidation on polycrystalline platinum catalysts in acidic electrolytes. Journal of Catalysis. 2011;**278**(2):181-188

[39] Braunchweig B, Hibbitts D, Neurock M, Wieckowski A. Electrocatalysis: A direct alcohol fuel cell and surface science perspective. Catalysis Today. 2013;**202**(1):197-209

[40] Gonzalez ER, Mota-Lima A. Catalysts for methanol oxidation. In: Direct Alcohol Fuel Cells. Netherlands, Dordrecht: Springer; 2014. pp. 33-62

[41] Morimoto Y, Yeager EB. CO oxidation on smooth and high area Pt, Pt-Ru and Pt-Sn electrodes. Journal of Electroanalytical Chemistry. 1998;**441**(1–2):77-81

[42] Vigier F, Coutanceau C, Hahn F, Belgsir EM, Lamy C. On the mechanism of ethanol electro-oxidation on Pt and PtSn catalysts: Electrochemical and in situ IR reflectance spectroscopy studies. Journal of Electroanalytical Chemistry. 2004;**563**(1):81-89

[43] Antoniassi RM, Oliveira Neto A, Linardi M, Spinacè EV. The effect of acetaldehyde and acetic acid on the direct ethanol fuel cell performance using $PtSnO_2$/C electrocatalysts. International Journal of Hydrogen Energy. 2013;**38**(27):12069-12077

[44] Wang H-F, Liu Z-P. Comprehensive mechanism and structure-sensitivity of ethanol oxidation on platinum: New transition-state searching method for resolving the complex reaction network. Journal of the American Chemical Society. 2008;**130**(33):10996-11004

[45] Kavanagh R, Cao XM, Lin WF, Hardacre C, Hu P. Origin of low CO_2 selectivity on platinum in the direct ethanol fuel cell. Angewandte Chemie (International Ed. in English). 2012;**51**(7):1572-1575

[46] Rousseau S, Coutanceau C, Lamy C, Lèger J-M. Direct ethanol fuel cell (DEFC): Electrical performances and reaction products distribution under operating conditions with different platinum-based anodes. Journal of Power Sources. 2006;**158**(1):18-24

[47] Colmati F, Antolini E, Gonzalez ER. Effect of temperature on the mechanism of ethanol oxidation on carbon supported Pt, PtRu and Pt_3Sn electrocatalysts. Journal of Power Sources. 2006;**157**(1):98-103

[48] Li H, Sun G, Cao L, Jiang L, Xin Q. Comparison of different promotion effect of PtRu/C and PtSn/C electrocatalysts for ethanol electro-oxidation. Electrochimica Acta. 2007;**52**(24):6622-6629

[49] Fatih K, Neburchilov V, Alzate V, Neagu R, Wang H. Synthesis and characterization of quaternary PtRuIrSn/C electrocatalysts for direct ethanol fuel cells. Journal of Power Sources. 2010;**195**(21):7168-7175

[50] Kim I, Han OH, Chae SA, Paik Y, Kwon S-H, Lee K-S, Sung Y-E, Kim H. Catalytic reactions in direct ethanol fuel cells. Angewandte Chemie (International Ed. in English). 2011;**50**(10):2270-2274

[51] Bach Delpeuch A, Maillard F, Chatenet M, Soudant P, Cremers C. Ethanol oxidation reaction (EOR) investigation on Pt/C, Rh/C, and Pt-based bi- and tri-metallic electrocatalysts: A DEMS and in situ FTIR study. Applied Catalysis B: Environmental. 2016; **181**:672-680

[52] Akhairi MAF, Kamarudin SK. Catalysts in direct ethanol fuel cell (DEFC): An overview. International Journal of Hydrogen Energy. 2016;**41**(7):4214-4228

[53] Watanabe M, Motoo S. Electrocatalysis by ad-atoms. Journal of Electroanalytical Chemistry and Interfacial Electrochemistry. 1975;**60**(3):275-283

[54] Vigier F, Coutanceau C, Perrard A, Belgsir EM, Lamy C. Development of anode catalysts for a direct ethanol fuel cell. Journal of Applied Electrochemistry. 2004;**34**(4): 439-446

[55] Vigier F, Rousseau S, Coutanceau C, Leger J-M, Lamy C. Electrocatalysis for the direct alcohol fuel cell. Topics in Catalysis. 2006;**40**(1–4):111-121

[56] Springer TE, Rockward T, Zawodzinski TA, Gottesfeld S. Model for polymer electrolyte fuel cell operation on reformate feed: Effects of CO, H_2 dilution, and high fuel utilization. Journal of the Electrochemical Society. 2001;**148**(1):A11-A23

[57] Franceschini EA, Corti HR. Applications and durability of direct methanol fuel cells. In: Direct Alcohol Fuel Cells. Netherlands, Dordrecht: Springer; 2014. pp. 321-355

[58] Olah GA, Goeppert A, Prakash GKS. Beyond Oil and Gas: The Methanol Economy. Wiley-VCH; 2006

[59] Carrette L, Friedrich KA, Stimming U. Fuel cells–Fundamentals and applications. Fuel Cells. 2001;**1**(1):5-39

[60] Kobayashi T, Otomo J, Wen C-J, Takahashi H. Direct alcohol fuel cell—relation between the cell performance and the adsorption of intermediate originating in the catalyst-fuel combinations. Journal of Power Sources. 2003;**124**(1):34-39

[61] Lèger J-M, Rousseau S, Coutanceau C, Hahn F, Lamy C. How bimetallic electrocatalysts does work for reactions involved in fuel cells?: Example of ethanol oxidation and comparison to methanol. Electrochimica Acta. 2005;**50**(25):5118-5125

[62] Liu H, Song C, Zhang L, Zhang J, Wang H, Wilkinson DP. A review of anode catalysis in the direct methanol fuel cell. Journal of Power Sources. 2006;**155**(2):95-110

[63] Ren X, Zelenay P, Thomas S, Davey J, Gottesfeld S. Recent advances in direct methanol fuel cells at Los Alamos National Laboratory. Journal of Power Sources. 2000;**86**:111-116

[64] Wang J, Wasmus S, Savinell RF. Evaluation of ethanol, 1-propanol, and 2-propanol in a direct oxidation polymer-electrolyte fuel cell. Journal of the Electrochemical Society. 1995;**142**(12):4218

[65] Friedl J, Stimming U. Model catalyst studies on hydrogen and ethanol oxidation for fuel cells. Electrochimica Acta. 2013;**101**:41-58

[66] Brouzgou A, Podias AKM, Tsiakaras P. PEMFCs and AEMFCs directly fed with ethanol: A current status comparative review. Journal of Applied Electrochemistry. 2013;**43** (2):119-136

[67] Song S, Tsiakaras P. Recent progress in direct ethanol proton exchange membrane fuel cells (DE-PEMFCs). Applied Catalysis B: Environmental. 2006;**63**(3):187-193

[68] Song S, Zhou W, Liang Z, Cai R, Sun G, Xin Q, Stergiopoulos V, Tsiakaras P. The effect of methanol and ethanol cross-over on the performance of PtRu/C-based anode DAFCs. Applied Catalysis B: Environmental. 2005;**55**(1):65-72

[69] Ekdharmasuit P, Therdthianwong A, Therdthianwong S. Anode structure design for generating high stable power output for direct ethanol fuel cells. Fuel. 2013;**113**:69-76

[70] Hitmi H, Belgsir EM, Lèger J-M, Lamy C, Lezna RO. A kinetic analysis of the electro-oxidation of ethanol at a platinum electrode in acid medium. Electrochimica Acta. 1994;**39** (3):407-415

[71] Iwasita T, Pastor E. A DEMS and FTIR spectroscopic investigation of adsorbed ethanol on polycrystalline platinum. Electrochimica Acta. 1994;**39**(4):531-537

[72] Wang H, Jusys Z, Behm RJJ. Ethanol electro-oxidation on carbon-supported Pt, PtRu and Pt_3Sn catalysts: A quantitative DEMS study. Journal of Power Sources. 2006;**154**(2):351-359

[73] Wang H, Jusys Z, Behm RJ. Ethanol electrooxidation on a carbon-supported Pt catalyst: reaction kinetics and product yields. The Journal of Physical Chemistry B. 2004;**108** (50):19413-19424

[74] Shao MH, Adzic RR. Electrooxidation of ethanol on a Pt electrode in acid solutions: in situ ATR-SEIRAS study. Electrochimica Acta. 2005;**50**(12):2415-2422

[75] Li G, Pickup PG. Analysis of performance losses of direct ethanol fuel cells with the aid of a reference electrode. Journal of Power Sources. 2006;**161**(1):256-263

[76] Antolini E. Catalysts for direct ethanol fuel cells. Journal of Power Sources. 2007;**170**(1):1-12

[77] Meyer M, Melke J, Gerteisen D. Modelling and simulation of a direct ethanol fuel cell considering multistep electrochemical reactions, transport processes and mixed potentials. Electrochimica Acta. 2011;**56**(11):4299-4307

[78] Weber AZ, Borup RL, Darling RM, Das PK, Dursch TJ, Gu W, Harvey D, Kusoglu A, Litster S, Mench MM, Mukundan R, Owejan JP, Pharoah JG, Secanell M, Zenyuk IV, Critical Review A. Of modeling transport phenomena in polymer-electrolyte fuel cells. Journal of the Electrochemical Society. 2014;**161**(12):F1254-F1299

[79] Gasteiger HA, Panels JE, Yan SG. Dependence of PEM fuel cell performance on catalyst loading. Journal of Power Sources. 2004;**127**(1–2):162-171

[80] Moran MJ, Shapiro HN. Fundamentals of Engineering Thermodynamics. 6th ed. New York, NY: John Wiley and Sons Inc.; 2009

[81] Mcbride BJ, Zehe MJ, Gordon S. NASA Glenn coefficients for calculating thermodynamic properties of individual species. NASA/TP—2002-211556. 2002

[82] Archer MD. Genesis of the Nernst equation. In: Electrochemistry, Past and Present. American Chemical Society; 1989. Chapter 8, pp. 115 -126

[83] Nernst W. Die elektromotorische Wirksamkeit der Jonen. Zeitschrift für Physikalische Chemie. 1889;**4**(1):129-181

[84] Nernst W. Zur Theorie umkehrbarer galvanischer Elemente. (vorgelegt von Hrn. von Helmholtz am 17. Januar). Sitzungsberichte der Preuss. Akad. der Wissenschaften zu Berlin. 1889;**1889**(1):83-85

[85] Tafel J. Über die Polarisation bei kathodischer Wasserstoffentwicklung. Zeitschrift für Physikalische Chemie. 1905;**50A**:641-712

[86] Fang Y-H, Liu Z-P. Tafel kinetics of Electrocatalytic reactions: From experiment to first-principles. ACS Catalysis. 2014;**4**(12):4364-4376

[87] Arrhenius S. Über die Dissociationswarme und den Einfluss der Temperatur auf den Dissociations grad der Elektrolyte. Zeitschrift für Physikalische Chemie. 1889;**4**(1):96-116

[88] Laidler KJ. The development of the Arrhenius equation. Journal of Chemical Education. 1984;**61**(6):494

[89] Back MH, Laidler KJ. Selected Readings in Chemical Kinetics. Pergamon; 1967

[90] Bard AJ, Faulkner LR. Electrochemical Methods: Fundamentals and Applications. New York: Wiley; 2001

[91] Atkins P, de Paula J. Atkins' Physical Chemistry. 9th ed. Oxford University Press; 2010

[92] Butler JAV. Studies in heterogeneous equilibria. Part II—The kinetic interpretation of the Nernst theory of electromotive force. Transactions of the Faraday Society. 1924;**19**:729-733

[93] Erdey-Gruz T, Volmer M. Zur theorie der wasserstoff überspannung. Zeitschrift für Physikalische Chemie. 1930;**150**:203

[94] Gileadi E. Electrode Kinetics for Chemists, Chemical Engineers, and Materials Scientists. New York: VCH Publishers; 1993

[95] Marcus RA. On the theory of oxidation-reduction reactions involving electron transfer. The Journal of Chemical Physics. 1956;**24**(5):966-978

[96] Marcus RA. Chemical and electrochemical electron-transfer theory. Annual Review of Physical Chemistry. 1964;**15**(1):155-196

[97] Marcus RA, Sutin N. Electron transfers in chemistry and biology. Biochimica et Biophysica Acta (BBA)-Reviews on Bioenergetics. 1985;**811**(3):265-322

[98] Langmuir I. The adsorption of gases on plane surfaces of glass, mica and platinum. Journal of the American Chemical Society. 1918;**40**(9):1361-1403

[99] Kauranen PS, Skou E, Munk J. Kinetics of methanol oxidation on carbon-supported Pt and Pt + Ru catalysts. Journal of Electroanalytical Chemistry. 1996;**404**(1):1-13

[100] Sundmacher K, Schultz T, Zhou S, Scott K, Ginkel M, Gilles ED. Dynamics of the direct methanol fuel cell (DMFC): Experiments and model-based analysis. Chemical Engineering Science. 2001;**56**(2):333-341

[101] Nordlund J, Lindbergh G. A model for the porous direct methanol fuel cells anode. Journal of the Electrochemical Society. 2002;**149**(9):A1107

[102] Shivhare MR, Allen RG, Scott K, Morris AJ, Martin EB. A kinetic model for the direct methanol fuel cell anode based on surface coverage. Journal of Electroanalytical Chemistry. 2006;**595**(2):145-151

[103] Shivhare MR, Jackson CL, Scott K, Martin EB. Simplified model for the direct methanol fuel cell anode. Journal of Power Sources. 2007;**173**(1):240-248

[104] Suresh NS, Jayanti S. Cross-over and performance modeling of liquid-feed polymer electrolyte membrane direct ethanol fuel cells. International Journal of Hydrogen Energy. 2011;**36**(22):14648-14658

[105] Sánchez-Monreal J, García-Salaberri PA, Vera M. A genetically optimized kinetic model for ethanol electro-oxidation on Pt-based binary catalysts used in Direct Ethanol PEM Fuel Cells. Journal of Power Sources. 2017;**363**:341-355

[106] Abd-El-Latif AA, Mostafa E, Huxter S, Attard G, Baltruschat H. Electrooxidation of ethanol at polycrystalline and platinum stepped single crystals: A study by differential electrochemical mass spectrometry. Electrochimica Acta. 2010;**55**(27):7951-7960

[107] Pramanik H, Basu S. Modeling and experimental validation of overpotentials of a direct ethanol fuel cell. Chemical Engineering and Processing Process Intensification. 2010;**49**(7):635-642

[108] Sousa R, dos Anjos DM, Tremiliosi-Filho G, Gonzalez ER, Coutanceau C, Sibert E, Lèger J-M, Kokoh KB. Modeling and simulation of the anode in direct ethanol fuels cells. Journal of Power Sources. 2008;**180**(1):283-293

[109] Zhang J, Wang JX, Adzic RR. Double-trap kinetic equation for the oxygen reduction reaction on Pt (111) in acidic media. The Journal of Physical Chemistry A. 2007;**111**(49):12702-12710

[110] Putz A, Moore M, Secanell M. Investigation of the ORR using the double-trap intrinsic kinetic model. Journal of the Electrochemical Society. 2013;**160**(6):F670-F681

[111] Sánchez-Monreal J, García-Salaberri PA, Vera M. A 1D + 1D model of direct ethanol fuel cells based on an optimized kinetic mechanism for ethanol electro-oxidation involving free and adsorbed intermediate species. ECS Transactions. 2017;**80**(8):95-104